Fuel 335 (2023) 127045

Contents lists available at ScienceDirect

Fuel

journal homepage: www.elsevier.com/locate/fuel

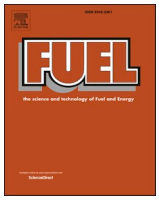

Full Length Article

Responses of trace elements and optical textures of ultra-deep pyrobitumen to hydrothermal alteration

Lianqiang Zhu [a,b], Zezhang Song [a,b,*], Xingwang Tian [c], Guangdi Liu [a,b], Dailin Yang [c], Wenzhi Wang [c], Gang Zhou [c], Wei Yan [c], Zhu Xiang [c], Zili Zhang [c], Qiang Li [a,b]

[a] State Key Laboratory of Petroleum Resources and Prospecting, China University of Petroleum, Beijing 102249, China
[b] College of Geosciences, China University of Petroleum, Beijing 102249, China
[c] Southwest Oil and Gas Field Company PetroChina, Chengdu 610041, China

ARTICLE INFO

Keywords:
Hydrothermal activity
Trace elements
Pyrobitumen
Ediacaran
Central sichuan basin

ABSTRACT

The hydrothermal activity in the Ediacaran Dengying (DY) Formation in central Sichuan has modified the reservoirs and paleo-oil reservoirs; however, these modifications are not specific due to the challenges in recovering the hydrothermal scale. This paper classified pyrobitumen in the DY Formation into five categories by optical textures and analyzed the physical structure and trace element composition of the different pyrobitumen using scanning electron microscope, reflectance, and trace elements. Finally, the responses of the trace element concentrations and optical textures of the pyrobitumen to hydrothermal alteration were discussed and used to restore the hydrothermal scale in the central Sichuan Basin. The results show that isotropic, fine-grained, medium-grained, coarse-grained mosaic, and fibrous pyrobitumen develop in the DY Formation. As the optical texture of the pyrobitumen changes from isotropic to mosaic to fibrous, the order degree of aromatic lamella in pyrobitumen gradually increases, the maturity, the maximum reflectance, and the bireflectance of pyrobitumen gradually increase. Except for isotropic pyrobitumen, anisotropic pyrobitumen is subject to varying degrees of hydrothermal alteration. The hydrothermal alteration on pyrobitumen is primarily in the form of material exchange, precipitating illite, salt, and barium-enriched minerals in pyrobitumen pores and enriching some elements (Ba, Cr, Nb, and Sr) in the pyrobitumen. As the optical texture changes from isotropic to mosaic to fibrous, the element enrichment degree gradually increases. Medium-grained mosaic, coarse-grained mosaic, and fibrous pyrobitumen are widely observed in central Sichuan. Therefore, hydrothermal modification on the DY reservoirs and paleo-oil reservoirs is not limited to the deep faults but widely develop in central Sichuan, and should be an essential part of the further study of hydrocarbon accumulation.

1. Introduction

Hydrothermal activity has been found in many sedimentary basins. The hydrothermal fluid significantly affected the formation of metal mineral deposits and oil and gas reservoirs and has become one of the hot spots in petroleum geology studies [27,30,12,19]. Hydrothermal modifications have been observed in hydrocarbon accumulation in many oil and gas fields, especially deep oil and gas, which has gradually become a research hotspot [36,42,54,29,25]. Hydrothermal fluid can cause dissolution or recrystallization of carbonate rocks to improve the porosity and permeability or promote the hydrothermal mineral filling to destroy existing pores. Hydrothermal modification on reservoirs is significant for oil and gas accumulation [4,18,17,20]. However, in the strata buried thousands of meters, it is challenging to restore the scale of hydrothermal activity only by the hydrothermal minerals developed in the drilling cores. Therefore, it is challenging to determine the extent of hydrothermal modification in deep oil and gas reservoirs.

The Sichuan Basin is at the southwest edge of the upper Yangtze plate, a valuable gas-enriched sedimentary basin in China [49,55,56,59,60]. The Anyue gas field in the central Sichuan Basin is one of the largest in the Sichuan Basin. Its primary production layer is Ediacaran-lower Cambrian, with a burial depth of > 4500 m [60,55,39]. Natural gas component, carbon isotope, and pyrobitumen distribution range analyses confirmed that the Anyue gas field was primarily derived from oil cracking, generating a large amount of pyrobitumen in the reservoir [22,33,34,43,60]. Current research proposes that the

* Corresponding author at: State Key Laboratory of Petroleum Resources and Prospecting, China University of Petroleum, Beijing 102249, China.
E-mail address: songzz@cup.edu.cn (Z. Song).

https://doi.org/10.1016/j.fuel.2022.127045
Received 9 October 2022; Received in revised form 18 November 2022; Accepted 1 December 2022
Available online 13 December 2022

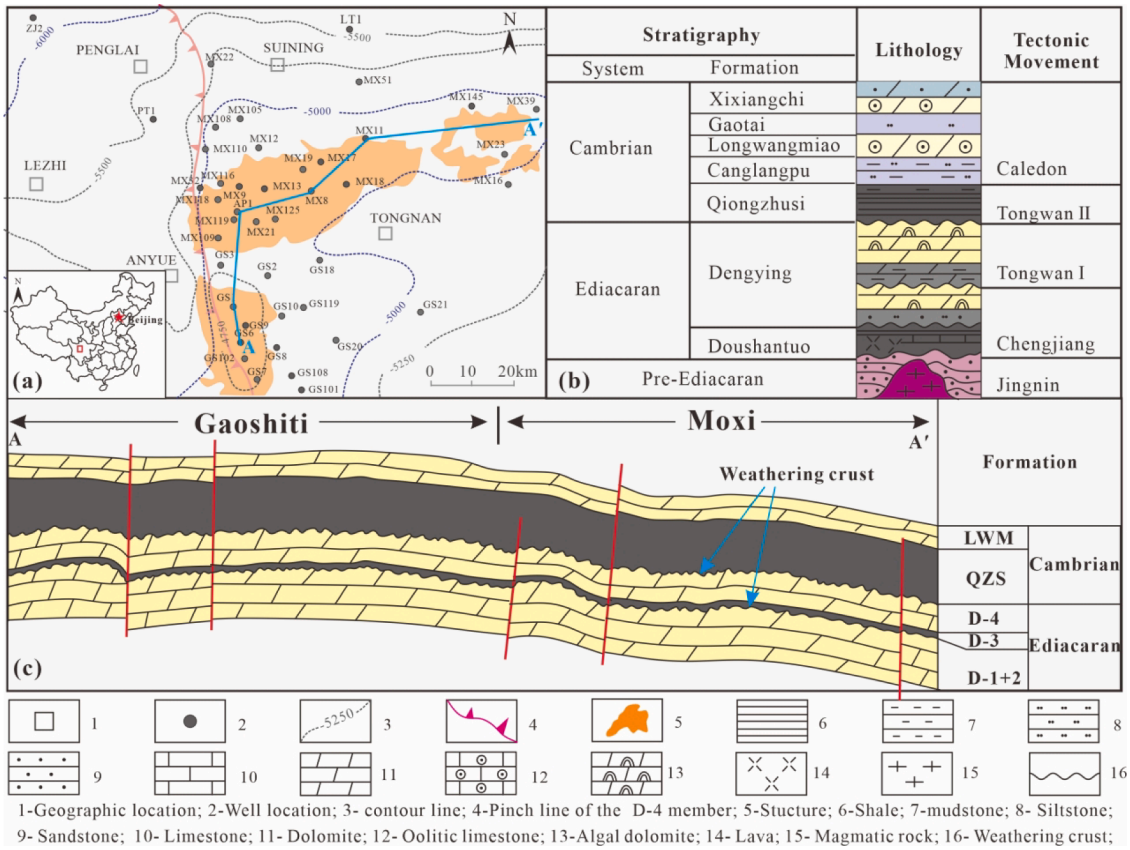

Fig. 1. Geological setting in central Sichuan. (a) The location of the study area and the primary wells; (b) The lithologic column in central Sichuan (modified from [47]; (c) The sectional view of the strata (modified from [62]).

hydrothermal activity in the Dengying (DY) Formation was related to the Emeishan mantle plume at the end of the Late Permian (259.1 Ma) [16,52]. Hydrothermal activity improved the physical properties of the DY Formation reservoir and provided adequate spaces for natural gas charging. Therefore, hydrothermal dolomite is the focus of gas exploration [18,9,10]. Furthermore, some studies also found that hydrothermal activity could have led to the oil cracking in the DY paleo-oil reservoir, a discovery for studying the hydrocarbon accumulation in the DY Formation [46,58,65]. However, due to the lack of effective methods to define the hydrothermal range, hydrothermal modification is challenging to determine and has not been paid enough attention in hydrocarbon accumulation studies [18,9,10]. Therefore, clarifying the hydrothermal scale could significantly influence understanding the hydrocarbon accumulation mechanism and exploration priorities.

Since the hydrothermal fluid led to oil cracking, the pyrobitumen cracked from oil could hold some traces of hydrothermal alteration. The hydrothermal fluid typically has a high temperature, and the fluid composition differs from the formation fluid. Therefore, the hydrothermal alteration on the pyrobitumen can occur on the maturity and the trace element composition. This paper classified the pyrobitumen in the DY Formation by optical texture and analyzed different pyrobitumens employing scanning electron microscopy (SEM), reflectance, and trace elements, to determine the relationship between the hydrothermal modification, optical texture, and trace element composition of pyrobitumen, and discuss the hydrothermal scale and the geological significance. The results have defined the hydrothermal scale, which has not been defined by predecessors, in the DY Formation in central Sichuan. This result can specify the range of hydrothermal modification on the reservoirs and paleo-oil reservoirs in a further study. In this study, the optical textures and trace elements of pyrobitumen were combined excellently to study the hydrothermal scale, providing a new method for hydrothermal study in the deep strata where pyrobitumen developed, and helping to specify the range of hydrothermal modification on oil and gas accumulation.

2. Geological setting

The Anyue gas field is in the gentle structural belt of the central Sichuan Basin and east of the axis of the Leshan-Longnvsi paleo-uplift [39]. Its primary reservoirs are the Ediacaran DY and Cambrian Longwangmiao (LWM) Formations (Fig. 1) [6,44,60]. DY Formation primarily comprises carbonate rocks deposited from rimmed platform facies and can be divided into four members from the bottom to the top: D-1, D-2, D-3, and D-4 (Fig. 1c) [6,44,53]. Affected by the Tongwan movement, numerous dissolution holes are developed in the D-2 and D-4 members, and a set of weathering crusts are developed on top of D-2 and D-4 (Fig. 1b and c) [21,22,32]. The LWM Formation primarily comprises granular dolomite deposited from gentle slope platform facies, and intergranular and dolomite intercrystalline pores are developed in the formation [5,53]. Large-scale paleo-oil reservoirs were developed in the DY and LWM formations in the central Sichuan Basin. Natural gas was derived from the oil cracking of the paleo-oil reservoirs, with a large amount of pyrobitumen remaining in the D-2, D-4, and LWM reservoirs after oil cracking [51,55,60,64].

3. Samples and experimental methods

3.1. Polished block preparation

Based on the core observation of approximately 40 drilling wells in the study area (Fig. 1a), the pyrobitumen-containing dolomite samples from the D-2, D-4, and LWM reservoirs were selected and placed into a

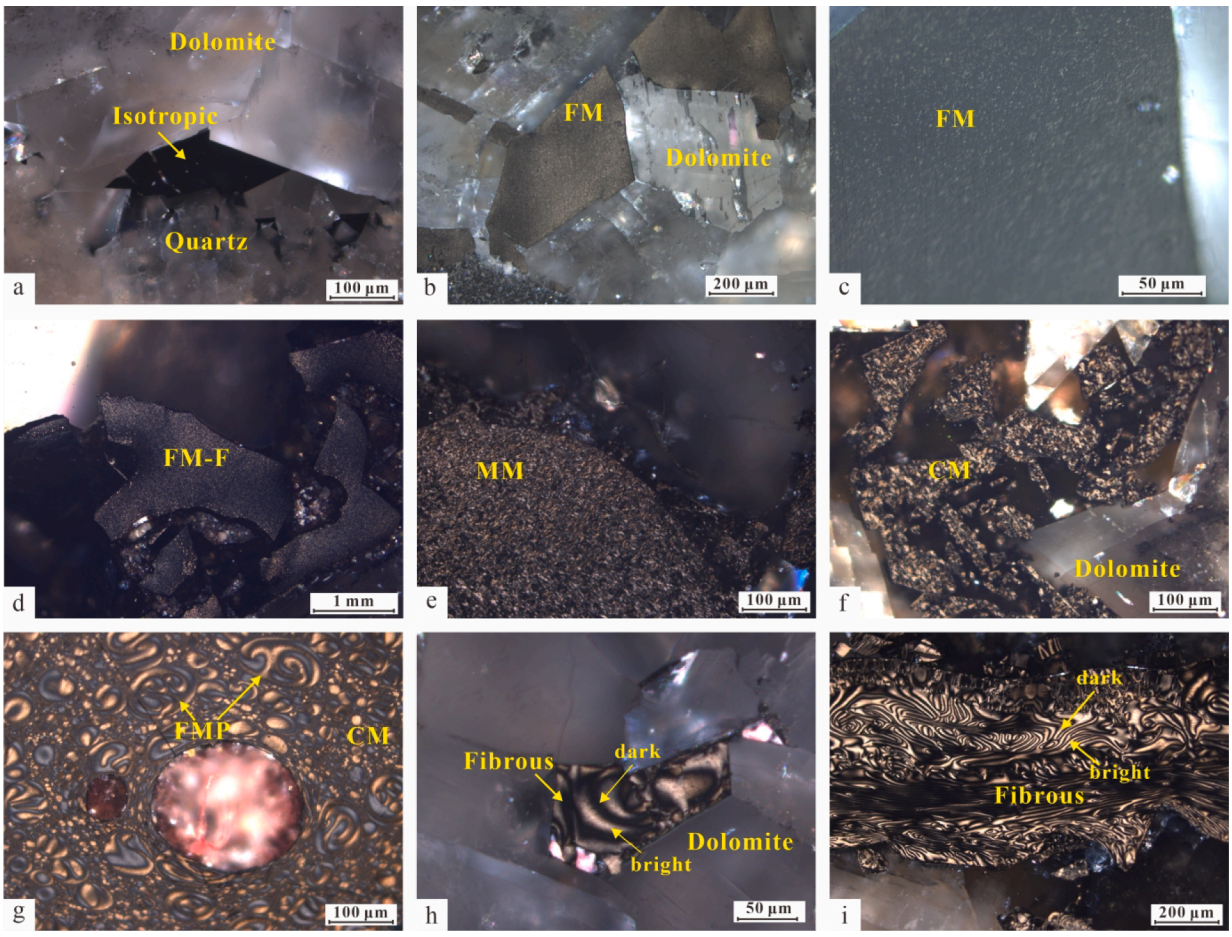

Fig. 2. Optical texture of the pyrobitumen in the DY Formation reservoir All photos were taken under reflected and cross-polarized light. (a) MX13, 4581.3 m, LWM, isotropic pyrobitumen; (b-c) MX145, 5822.15 m, D-4, (c) is the enlarged view of (b), FM pyrobitumen filled in the intergranular pore of dolomite;(d) PT1, 5733.89 m, D-2, FM pyrobitumen alternatively developed with fibrous pyrobitumen in (i); (e) MX125, 5383.79 m, D-4, MM pyrobitumen; (f) MX116, 5125.72 m, D-4, CM pyrobitumen filled in the intergranular pore of dolomite; (g) GS20, 5183.47 m, D-4, CM pyrobitumen with bubbles, some mesophase spheres in the pyrobitumen has fused; (h) PT1, 5786.73 m, D-2, fibrous pyrobitumen with dark and bright bonds filled in the intergranular pore of dolomite; (i) GS6, 5367.00 m, fibrous pyrobitumen with dark and bright bonds;

mold containing a mixture of epoxy resin, ethylenediamine, and dioctyl phthalate. After this mixture solidified, it was polished for the optical observation of pyrobitumen and reflectance measurement.

3.2. Pyrobitumen sample preparation

Based on the observation of numerous rock thin sections, the drilling cores containing the pyrobitumen with a single optical texture were selected for pyrobitumen powder preparation. The pyrobitumen sampling range was controlled within a small area where the related thin sections were ground and the pyrobitumen sample weight was controlled within 200 mg. Therefore the optical texture of the obtained pyrobitumen was consistent with that of the thin section, and the relative amount of the corresponding texture was close to 100 %.

The pyrobitumen-containing dolomite blocks were first broken into 3–5 mm pieces to obtain pure reservoir pyrobitumen samples. The pyrobitumen particles that separated from the rock sample were selected using wooden tweezers. The attached mineral fragments, such as dolomite and quartz on the pyrobitumen surface, were removed using a wooden tool under a 10 × microscope. The pyrobitumen particles were then placed into a small beaker filled with deionized water, cleared under 50 Hz ultrasonic waves for 1 h, and dried in a drying oven. Finally, the pyrobitumen samples were ground into the 200-mesh powder using an agate mortar.

Some pyrobitumen powder samples were placed into a beaker containing hydrochloric acid with a concentration of 75 % and washed for 1 h under 50 Hz ultrasonic vibration. The washed samples were filtered using filter papers and flushed repeatedly using deionized water. The process was repeated three times, and the samples were finally dried in a drying oven. This treatment removed the authigenic minerals filled in the pyrobitumen pores.

3.3. SEM sample preparation

The pyrobitumen particles obtained from the dolomite were knocked using a small hammer to show a fresh surface. The pyrobitumen was glued to the metal plate with black conductive tape. The samples were gilded using an SCD500 Ion sputtering instrument for SEM observation.

3.4. Experimental methods

3.4.1. Polished block observation

The optical texture of pyrobitumen was observed at the State Key Laboratory of Oil and Gas Resources and Exploration of China University of Petroleum (Beijing), using a Leica DM 4500P polarized microscope equipped with a DFC450C camera.

3.4.2. Reflectance measurement

The China University of Petroleum, Beijing, completed the pyrobitumen reflectance measurements. The reflectance was measured under

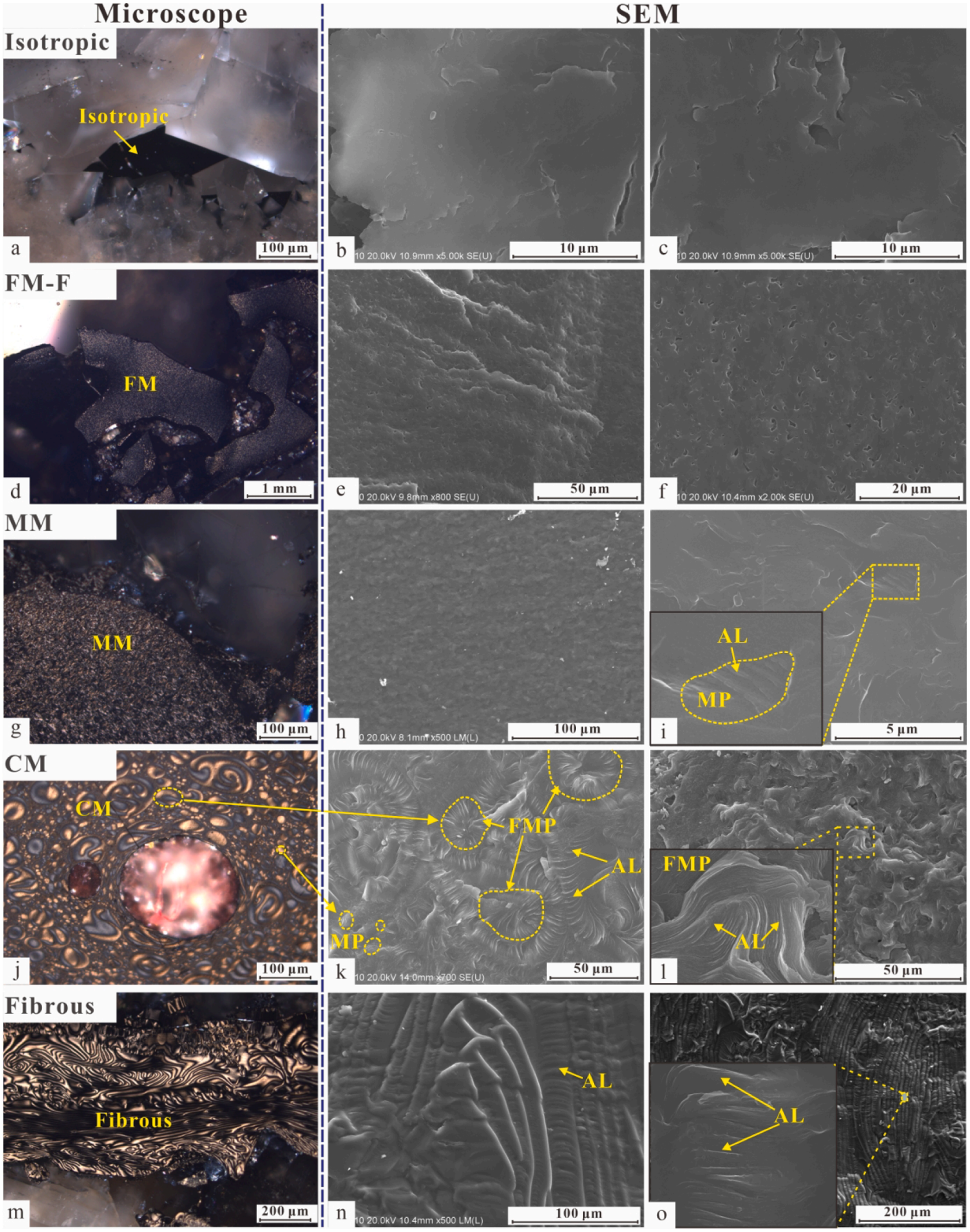

Fig. 3. Scanning electron microscopy (SEM) photos of pyrobitumen with different optical textures (a–c) MX13, 4581.3 m, LWM, the internal structure is uniform, and no mesophase spheres precipitate in the isotropic pyrobitumen; (d–f) PT1, 5733.89 m, D-2, bubbles are observed in the FM pyrobitumen while mesophase spheres are too small to observe; (g–i) MX125, 5383.79 m, D-4, many mesophase spheres are observed in the pyrobitumen, and aromatic lamella (AL) is observed in some mesophase spheres; (j–l) numerous mesophase spheres with apparent and orderly arranged AL are observed in the CM pyrobitumen; some fused mesophase spheres (FMP) exhibit curved AL; (m–o) GS6, 5367.00 m, several orderly arranged AL were observed in the fibrous pyrobitumen.

oil immersion (1.518 refractive index oil) using a Leica microscope equipped with a CRAIC microscope photometer and calibrated with a cubic-zirconia reference (R_o = 3.08 %) and a strontium titanate reference (R_o = 5.39 %). During the measurement, the microscope stage was rotated 360°, and the reflectance was measured every 10° to obtain the maximum and minimum reflectance ($R_{o\text{-}max}$ and $R_{o\text{-}min}$, respectively) at a measured point [23,24]. Every reflectance test area was approximately 1 μm^2. The bireflectance value was calculated as the difference between $R_{o\text{-}max}$ and $R_{o\text{-}min}$.

3.4.3. SEM observation

The pyrobitumen SEM observation was conducted at the Materials and Microstructure Laboratory of the China University of Petroleum, using a SU8010 cold field emission SEM with an energy dispersive X-ray spectrometer (EDS). Photos were taken under vacuum at 20 kV and a working distance of approximately 10.0 mm. The weight and atomic percentage of elements measured by EDS were estimated using the normalized nonstandard EDAX-ZAF quantitative method.

3.4.4. Trace element analysis

Pyrobitumen trace elements were analyzed at the Beijing Institute of Geology of Beijing Nuclear Industry using a Thermo Scientific Element XR inductively coupled plasma mass spectrometer, and 10-ng Rh was used as the online internal standard in the experiment. The repeated laboratory measurement of standard rock samples controlled the analysis accuracy, and the trace element analysis error was less than 5 %. The Post-Archean Australian Shale (PAAS) was used for standardization to eliminate the odd–even effect of trace elements.

4. Results

4.1. Optical texture of pyrobitumen

Pyrobitumen in the DY Formation can be divided into five categories according to its optical texture: isotropic, fine-grained mosaic (FM), medium-grained mosaic (MM), coarse-grained mosaic (CM), and fibrous [13,28,31,41] (Fig. 2). The isotropic pyrobitumen has no anisotropic particles inside, showing a uniform texture (Fig. 2a). FM pyrobitumen has anisotropic particles of less than one micron, performing weak anisotropy under the microscope (Fig. 2b–d). MM and CM pyrobitumens have larger anisotropic particles (Fig. 2e–g) with diameters of 1–5 and > 5 μm, respectively [30]. The fibrous pyrobitumen shows an alternating texture of dark and bright bands (Fig. 2h and i), which could result from the collapse of bubbles formed from volatile components [40,36,30].

In the study, some FM and MM pyrobitumens (abbreviated as FM-F and MM-F, respectively, in the following text) were found alternatively developed with fibrous pyrobitumen (Fig. 2d). In previous studies, we have confirmed that these mosaic pyrobitumen shows a similar hydrothermal modification to fibrous pyrobitumen through thermogravimetric and nuclear magnetic analysis [58].

4.2. Physical structure of pyrobitumen

The pyrobitumens with different optical textures exhibit different structures under the SEM (Fig. 3). The internal surface of isotropic pyrobitumen is uniform, with a smooth fractured surface (Fig. 3a–c). However, the mesophase spheres can be observed in FM, MM, CM, and fibrous pyrobitumens (Fig. 3d–o). Isolated and fused mesophase spheres can be observed in the CM and fibrous pyrobitumens. The aromatic lamellae in these mesophase pyrobitumens are developed and neatly arranged (Fig. 3j–o). These aromatic lamellae are polycondensate from polycyclic aromatic compounds in pyrobitumen at a high temperature (over 300 °C) [3,40,26,14,48,7,38].

Table 1
Reflectance of pyrobitumen with different optical textures.
Note: $R_{o\text{-}max}$ = maximum reflectance; $R_{o\text{-}min}$ = minimum reflectance; BR_o = bireflectance value.

Well	Depth (m)	Formation	Optical texture	$R_{o\text{-}max}$ (%)	$R_{o\text{-}min}$ (%)	BR_o (%)
MX13	4581.32	LWM	Isotropic	2.78	2.63	0.15
				2.45	2.42	0.03
				2.37	2.15	0.22
				2.70	2.35	0.35
PT1	5733.89	D-2	FM-F	3.75	2.40	1.35
				3.86	2.42	1.44
				3.92	2.38	1.54
				3.99	2.45	1.54
				4.02	2.30	1.72
				3.93	2.10	1.83
				3.79	2.01	1.78
MX125	5334.72	D-4	MM	6.09	1.52	4.56
				5.35	1.63	3.72
				5.22	1.58	3.64
				5.94	1.44	4.50
GS124	5547.57		CM	8.52	1.39	7.13
				7.11	1.36	5.75
				7.41	1.60	5.81
				7.72	1.30	6.42
				8.18	1.52	6.66
				8.06	1.47	6.59
GS6	5367.00		Fibrous	8.67	0.88	7.79
				7.53	0.58	6.95
				8.17	0.77	7.40
GS7	5260.50		Fibrous	9.35	0.14	9.21
				9.12	0.35	8.77
				9.12	0.34	8.78
				9.03	0.23	8.80
				8.86	0.32	8.54

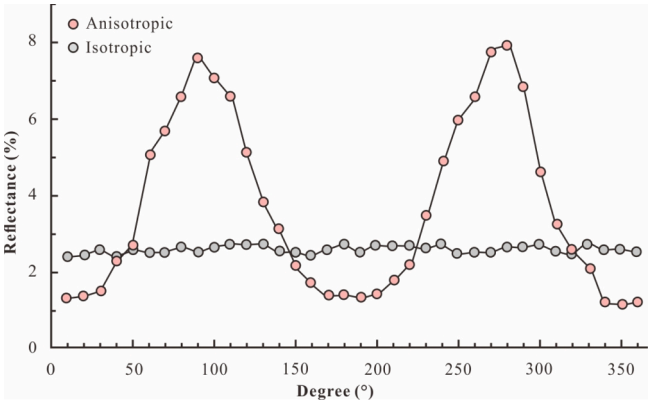

Fig. 4. The changing trend of pyrobitumen reflectance with the platform angle The reflectance of isotropic pyrobitumen alters weakly as the platform angle increases; the reflectance of anisotropic pyrobitumen exhibits the trend of increase → decrease → increase → decrease as the platform angle increases;

4.3. Reflectance of pyrobitumen

Isotropic pyrobitumen performs optical isotropy. The $R_{o\text{-}max}$ values of pyrobitumen range from 2.37 % to 2.78 %, whereas the $R_{o\text{-}min}$ values range from 2.15 % to 2.63 %. The bireflectance values are lower than 0.5 %, and the reflectances at different angles are similar (Table 1, Fig. 4). The reflectance of anisotropic pyrobitumen performs bireflectance. As the microscope stage angle alters, the reflectance of pyrobitumen exhibits regular changes (Fig. 4). As the optical texture of pyrobitumen changes as isotropic → FM → MM → CM → fibrous, the $R_{o\text{-}max}$ value of pyrobitumen gradually increases, the $R_{o\text{-}min}$ value gradually decreases, and the bireflectance value gradually increases, indicating an increasing degree of anisotropy (Table 1).

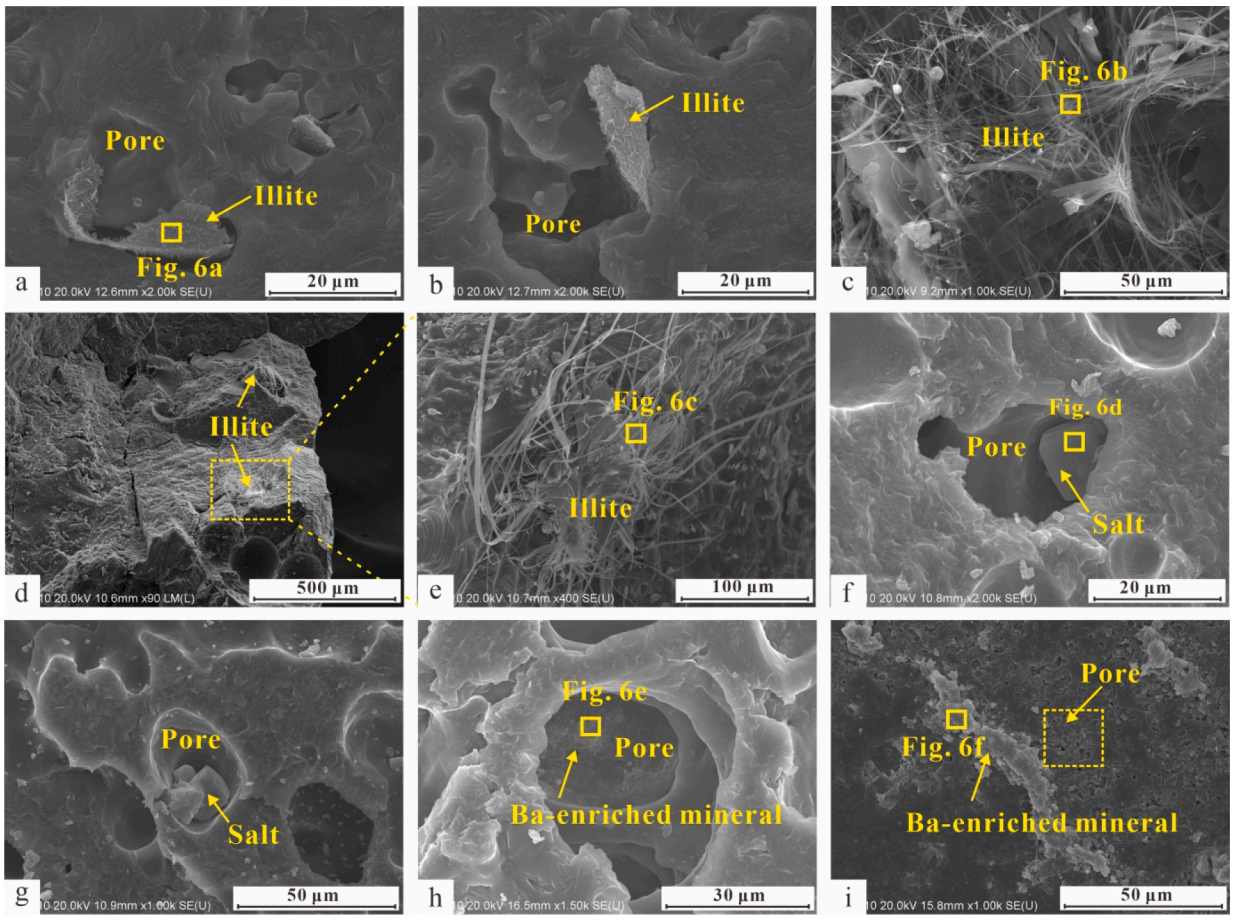

Fig. 5. SEM photos of minerals filled in the pyrobitumen pores The positions in the red box of the figures were analyzed by energy spectrum, and the energy spectrogram is shown in Fig. 6. (a, b) MX116, 5125.72 m, D-4, authigenic flaky illite is filled in the pores inside the pyrobitumen; (c) GS124, 5547.6 m, D-4, authigenic ribbon illite is filled in the pores inside the pyrobitumen; (d, e) GS7, 5293.4 m, D-4, authigenic ribbon illite is filled in the pores inside the pyrobitumen; (f, g) ZJ2, 6546.27 m, D-2, cubic salt crystals are filled in the pores inside the pyrobitumen; (h) ZJ2, 6547.22 m, D-2, some amorphous barium-enriched minerals are attached to the pore wall; (i) PT1, 5746.51 m, D-2, the banded barium-enriched minerals along the high porosity of pyrobitumen. (For interpretation of the references to colour in this figure legend, the reader is referred to the web version of this article.)

4.4. Minerals filled in the pyrobitumen pores

The SEM photos show that the pores are developed in the DY pyrobitumen and filled with some authigenic minerals (Fig. 5). Two illite shapes are observed in the pores (lamellar and ribbon), and primarily comprise O, Mg, Al, Si, and K. Unlike ribbon illite, lamellar illite also contains some V, Cr, and other elements (Fig. 5a–e, 6a–c). The pyrobitumen pores also contain some regular cubic minerals. The EDS result confirms that this mineral is salt primarily somprising Na and Cl (Fig. 5f, g, 6d). Some irregular minerals are found in the pyrobitumen pore walls, containing high concentrations of Ba and nemerous S, O, Ca, and other elements (Fig. 5h, i, 6e, f).

4.5. Trace elements of pyrobitumen

The trace element concentrations in pyrobitumen before hydrochloric acid treatment ranged from 413.57 to 25925.32 μg/g (mean value of 5190.14 μg/g). The trace element concentrations in pyrobitumens with different textures noticeably differed (Table 2, 3). However, the trace element concentrations in the pyrobitumen after hydrochloric acid treatment had a narrow range from 185.37 to 772.16 μg/g (mean value of 426.73 μg/g), lower than that of pyrobitumen before hydrochloric acid treatment. Not all elements significantly decreased after treatment. The Ba, Cr, Sr, Nb, Zn, and U concentrations noticeably decreased, while other elements had not changed much, especially V and Ni (Fig. 7).

5. Discussion

5.1. Relationship between optical texture and maturity

Temperature significantly affects the optical texture of pyrobitumen. Due to the molecular characteristics of aromatic hydrocarbon, the appropriate temperature for thermal polycondensation reaction is generally 350–500 °C. If the reaction temperature is below 300 °C, the mesophase spheres cannot form, and pyrobitumen shows an isotropic texture [35,7,48,8,38]. When the temperature exceeds 300 °C, mesophase spheres gradually form with the maturity increase. Through growing up and mutual fusing, an anisotropic nematic liquid crystal structure is formed [3,15,1,2,45]. The SEM photos of pyrobitumen show that the fractured surface of isotropic pyrobitumen is uniform, and no mesophase spheres precipitate, indicating that the formation temperatures of these pyrobitumen are low. Therefore, the aromatic compounds in the pyrobitumen do not polycondense yet. The optical characteristics of this type of pyrobitumen show noticeable isotropy, and the reflectivity does not change as the platform angle changes. With the maturity increase, the aromatic compounds in the pyrobitumen polycondense to form mesophase spheres, and the pyrobitumen performs optical anisotropy (Fig. 3). The sizes of mesophase spheres in FM pyrobitumen are too small (<1 μm) to observe under the microscope, whereas the

Table 2
Trace element concentrations of reservoir pyrobitumen samples not treated by hydrochloric acid (standardized using PAAS, some trace elements were published in Zhu et al., 2022 [57]).

Well	Formation	Depth	Texture	Trace elements																
				Ba	V	Cr	Co	Ni	Cu	Zn	Ga	Pb	Th	Sr	Zr	Nb	Y	U	Li	Mo	Sc
PT1	D-2	5780.74	Fibrous	39.045	1.127	0.265	0.015	1.153	0.139	0.249	0.313	2.010	0.011	0.865	0.004	0.011	0.022	0.035	0.007	3.430	0.006
		5778.2	Fibrous	39.020	0.727	0.395	0.017	0.987	0.125	0.207	0.277	5.600	0.010	0.915	0.006	0.017	0.023	0.033	0.007	5.220	0.011
		5741.06	FM-MM-F	20.520	1.233	0.220	0.032	2.000	2.160	0.166	0.032	4.705	0.006	0.595	0.004	0.014	0.014	0.020	0.004	1.380	0.010
		5733.89	FM-F	8.117	1.420	0.132	0.021	2.091	0.808	5.282	0.045	37.700	0.006	0.260	0.002	0.008	0.006	0.016	0.002	1.730	0.008
		5733.28	FM-F	4.703	0.571	0.491	0.018	1.636	0.035	1.306	0.034	3.175	0.005	0.217	0.004	0.017	0.026	0.053	0.013	1.980	0.011
		5730.03	MM-F	7.820	0.365	0.265	0.039	0.615	22.620	/	3.085	8.000	0.011	0.244	0.005	0.024	0.012	0.028	0.005	0.489	0.009
ZJ2		6553.56	MM-CM	1.252	0.428	0.042	0.005	1.784	0.014	0.208	0.126	0.610	0.002	0.091	0.003	0.002	0.003	0.007	0.020	0.388	0.008
		6551.45	MM-CM	5.085	0.462	0.077	0.014	1.873	0.049	1.435	0.119	1.605	0.001	0.267	0.005	0.003	0.006	0.026	0.020	0.305	0.041
		6547.22	FM-MM	0.220	0.587	0.054	0.010	1.927	0.012	0.142	0.119	1.335	0.005	0.096	0.003	0.004	0.009	0.025	0.018	0.684	0.011
		6546.48	FM	4.142	0.662	0.047	0.012	2.073	0.021	0.110	0.130	3.705	0.003	0.198	0.002	0.003	0.007	0.012	0.068	1.630	0.009
		6546.27	MM-CM	2.592	0.880	0.059	0.004	2.018	0.011	0.052	0.145	2.300	0.001	0.142	0.001	0.003	0.002	0.014	0.031	1.090	0.008
MX26	LWM	4913.54	MM	1.762	0.827	0.185	0.005	0.524	0.612	0.036	0.154	0.312	0.001	0.086	0.002	0.002	0.002	0.005	0.014	0.178	0.030
		4910.3	MM	5.020	0.853	0.288	0.030	0.625	0.328	0.028	0.119	13.950	0.007	0.422	0.007	0.009	0.013	0.047	0.067	0.481	0.032
MX56		4968.58	FM	1.902	0.993	0.224	0.008	1.436	0.018	0.017	0.073	0.215	0.010	1.075	0.009	0.002	0.004	0.055	0.089	0.292	0.053
		4966.13	FM	0.482	1.380	0.304	0.116	2.000	0.226	0.048	0.206	5.750	0.140	0.780	0.099	0.142	0.034	1.513	0.071	5.340	0.083
MX13		4581.32	Isotropic	0.192	1.780	0.027	0.005	2.073	0.007	0.059	0.019	1.725	0.001	0.011	0.002	0.000	0.000	0.007	0.004	1.450	0.002
MX39	D-4	5307.16	MM	2.057	1.820	0.158	0.023	3.345	0.196	1.424	0.100	2.515	0.003	0.166	0.003	0.006	0.004	0.432	0.018	6.130	0.006
		5301.02	MM	2.197	1.640	0.187	0.010	2.527	0.061	0.744	0.072	2.170	0.002	0.119	0.002	0.004	0.004	0.044	0.026	2.800	0.007
		5298.21	MM	4.837	1.487	0.319	0.020	2.418	0.054	0.789	0.069	1.700	0.005	0.234	0.006	0.009	0.008	0.416	0.073	5.640	0.008
		5284.68	MM	2.595	1.887	0.175	0.015	3.036	0.058	0.498	0.061	2.410	0.004	0.132	0.002	0.006	0.008	0.145	0.052	3.600	0.009
		5267.18	MM	0.039	2.013	0.074	0.009	2.727	0.008	0.218	0.067	0.535	0.001	0.019	0.001	0.000	0.003	0.055	0.006	4.340	0.007
MX108		5330.34	FM	0.654	1.627	0.312	0.036	2.218	0.044	0.047	0.156	0.085	0.003	0.144	0.014	0.006	0.039	4.000	0.021	7.010	0.046
MX116		5125.72	CM	15.095	2.100	0.352	0.031	2.764	0.072	1.318	0.077	0.037	0.022	0.505	0.005	0.006	0.015	0.032	0.019	3.260	0.050
MX125		5334.72	FM	0.200	1.427	0.183	0.012	1.927	0.011	0.085	0.060	0.013	0.001	0.117	0.001	0.001	0.010	0.008	0.026	2.030	0.038

Table 3
Trace element concentrations of pyrobitumen samples treated by hydrochloric acid (standardized using PAAS).

Well	Formation	Depth	Texture	Trace elements																
				Ba	V	Cr	Co	Ni	Cu	Zn	Ga	Pb	Th	Sr	Zr	Nb	Y	U	Li	Mo	Sc
MX125	D-4	5383.79	MM	0.091	1.193	0.056	0.007	1.982	0.011	0.079	0.016	3.980	0.002	0.028	0.001	0.001	0.001	0.014	0.010	1.690	0.004
		5334.72	MM	0.007	1.287	0.024	0.007	1.927	0.009	0.079	0.010	10.700	0.000	0.059	0.001	0.001	0.009	0.004	0.024	2.120	0.005
			FM-MM	0.011	1.127	0.023	0.006	1.836	0.013	0.090	0.016	6.750	0.000	0.016	0.001	0.000	0.004	0.008	0.005	2.030	0.002
GS20		5184.44	CM	0.309	0.820	0.027	0.004	1.424	0.008	0.140	0.004	0.630	0.001	0.046	0.005	0.001	0.006	0.023	0.005	0.543	0.003
		5192.45	Fibrous	0.054	1.373	0.020	0.005	2.182	0.005	0.053	0.027	1.425	0.000	0.028	0.001	0.000	0.001	0.040	0.006	5.820	0.001
		5184.95	CM	0.021	0.753	0.020	0.003	1.311	0.006	0.054	0.002	1.110	0.000	0.009	0.001	/	0.002	0.003	0.002	0.252	0.003
		5182.27	CM-Fibrous	0.012	0.673	0.017	0.002	1.111	0.005	0.035	0.003	0.352	0.001	0.006	0.001	0.000	0.000	0.014	0.003	0.170	0.002
		5196.71	MM	0.009	0.807	0.018	0.003	1.207	0.003	0.043	0.009	0.485	0.002	0.013	0.001	0.000	0.003	0.030	0.004	0.325	0.003
		5183.47	CM	0.020	0.907	0.021	0.004	1.409	0.006	0.080	0.007	1.685	0.001	0.043	0.001	0.000	0.013	0.003	0.004	0.181	0.001
		5183.3	CM	0.063	0.793	0.022	0.003	1.253	0.008	0.091	0.005	1.125	0.000	0.024	0.001	0.000	0.002	0.002	0.004	0.211	0.001
GS6		5367.16	Fibrous	0.075	1.053	0.021	0.004	1.200	0.014	0.045	0.021	0.610	0.000	0.039	0.001	0.000	0.002	0.007	0.004	7.260	0.001
MX11		5487.29	MM-CM	0.012	1.293	0.023	0.004	1.927	0.008	0.048	0.008	4.370	0.001	0.005	0.001	0.000	0.001	0.015	0.010	11.500	0.002
MX116		5125.72	CM	0.094	2.060	0.023	0.014	2.691	0.015	0.121	0.016	4.115	0.000	0.009	0.001	0.000	0.001	0.007	0.007	3.030	0.003
GS101		5250	Fibrous	0.014	0.960	0.012	0.002	1.084	0.003	0.031	0.022	0.490	/	0.003	0.000	0.000	/	0.002	0.004	2.170	0.001
PT1	D-2	5733.89	FM-MM	0.105	1.307	0.030	0.006	1.964	0.220	0.042	0.030	9.200	0.000	0.017	0.001	0.001	0.000	0.005	0.004	1.920	0.002
MX205	LWM	4602.48	FM	0.506	1.520	0.029	0.005	1.455	1.686	0.068	0.222	1.180	0.001	0.039	0.001	0.000	0.001	0.017	0.005	0.517	/
MX12		4629.54	CM	0.116	1.687	0.024	0.007	1.545	0.928	0.094	0.078	0.845	0.001	0.083	0.001	0.000	0.003	0.010	0.004	1.000	0.001
		4633.81	FM-MM	0.118	1.513	0.040	0.006	1.500	0.025	0.232	0.033	0.670	0.001	0.018	0.001	0.000	0.001	0.006	0.005	0.652	0.003

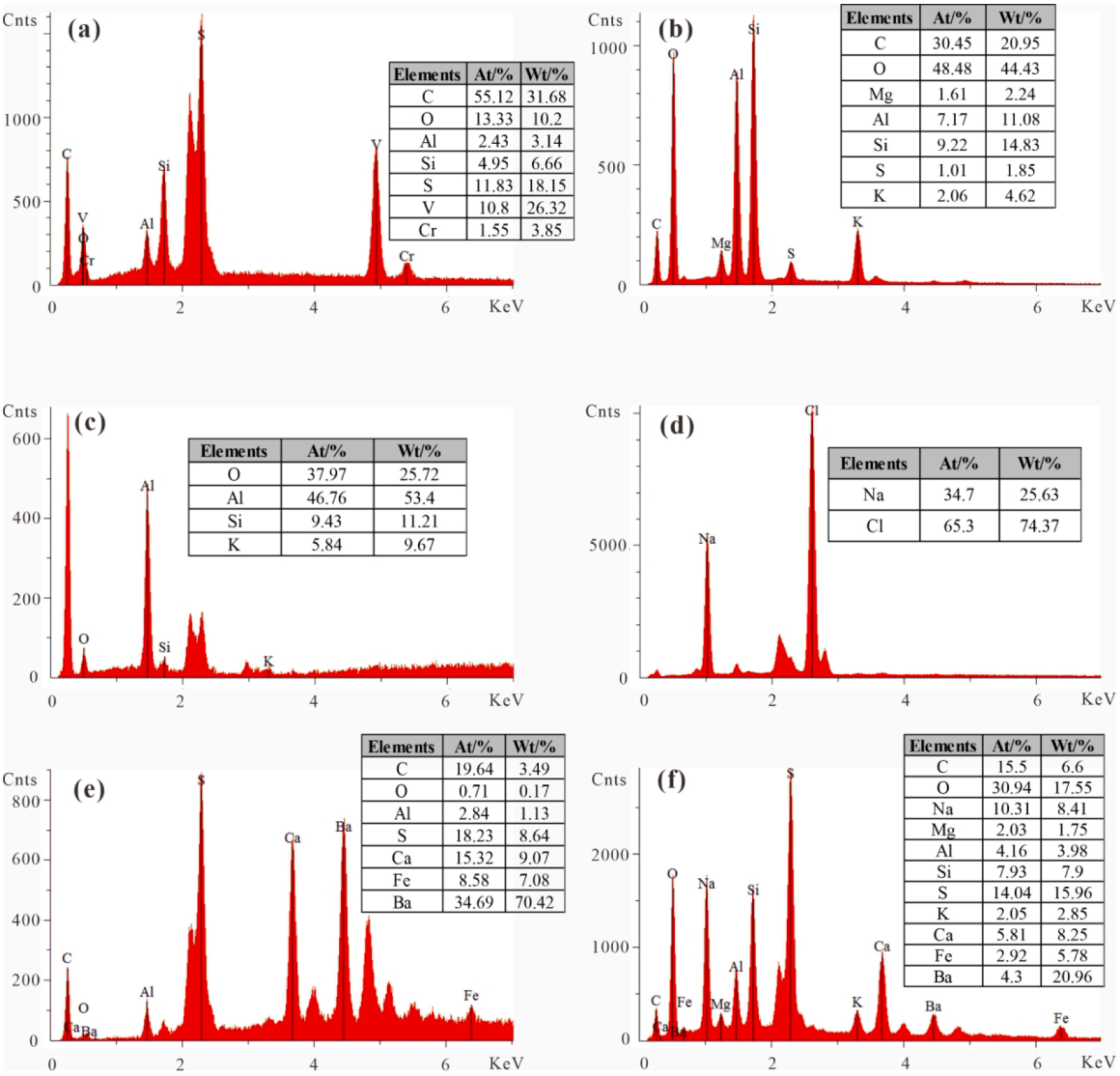

Fig. 6. EDS spectra of the authigenic minerals filled in the pores of pyrobitumen The letters of EDS spectra correspond to the red box displayed in Fig. 5. (a) The letters correspond to Fig. 5a, flaky illite; (b) Correspond to Fig. 5c, ribbon illite; (c) Correspond to Fig. 5e, ribbon illite; (d) Correspond to Fig. 5f, cubic salt crystal; (e) Correspond to Fig. 5h, barium-enriched minerals; (f) Correspond to Fig. 5i, barium-enriched minerals; (For interpretation of the references to colour in this figure legend, the reader is referred to the web version of this article.)

mesophase spheres in the MM pyrobitumen show apparent shapes. The orderly stacked aromatic lamella can be observed inside some mesophase spheres. These aromatic lamellae have a limited specific order degree (Fig. 3d–i). The mesophase spheres in the CM pyrobitumen are very developed, and some mesophase spheres have fused. The order degree and orientation of the aromatic lamellae improve (Fig. 3j–l). The aromatic lamellae inside the fibrous pyrobitumen are arranged orderly, with the highest order degree and best orientation (Fig. 3m–o). As the order degree and orientation of aromatic lamellae gradually improve, the optical texture of the pyrobitumen changes regularly as isotropic → FM → MM → CM → fibrous, and its bireflectance increases gradually (Table 1, Fig. 8). The optical texture of pyrobitumen could be the mapping of its internal structure. As the order degree and orientation of aromatic lamellae improve, the pyrobitumen maturity gradually increases, and the optical texture regularly changes. This result is consistent with that obtained through thermogravimetry and nuclear magnetic resonance analysis [58]. The pyrobitumen reflectance is closely related to its optical texture. As the order degree and orientation of the aromatic lamellae gradually improve, the $R_{o\text{-}max}$ and bireflectance of pyrobitumen increase progressively (Table 1, Fig. 8).

5.2. *Trace element enrichment*

The SEM and EDS results confirm that some illite, salt, and barium-enriched minerals are filled in the pyrobitumen pores (Figs. 5 and 6). These barium-enriched minerals contain high concentrations of S, O, Ba, and Na, which could be a mixture of barite, mirabilite, salt, and other minerals (Fig. 6e, f). Illite and salt show a high idiomorphic degree, precipitated in the pyrobitumen pores (Fig. 5a–g). However, DY and LWM reservoirs in the study area comprise carbonate, lacking the potassium-enriched condition for illite precipitation. Therefore, illite is rarely found in the reservoir. Furthermore, the salinity of the general formation fluid is only 8 wt% NaCl, which does not reach the concentration for salt precipitation. The fluid from which these minerals precipitate differs from the formation fluid at that time. The Ba enrichment in the reservoir is typically considered to be the drilling mud pollution. Considering that the samples were cleared by deionized water and the barium-enriched minerals are found filling the pyrobitumen pores without other symbiotic clastic materials contained in the mud, these barium-enriched minerals are suggested to be authigenic in the pores. Gao et al. [11] found some barium-enriched minerals in the DY

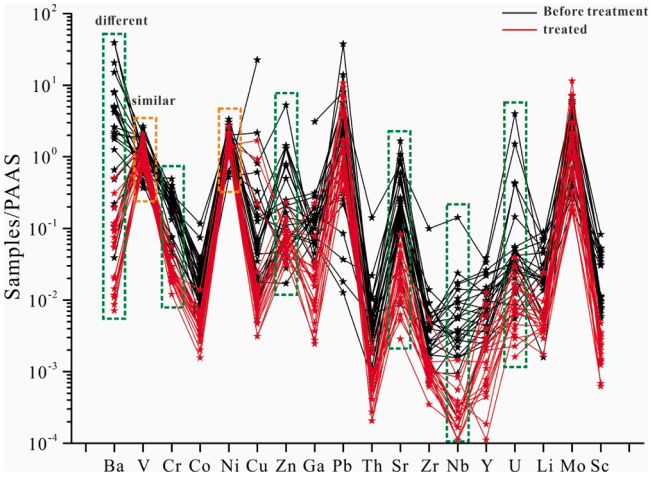

Fig. 7. Trace element distribution characteristic of pyrobitumen The distribution trends of trace elements in the pyrobitumen samples before and after hydrochloric acid treatment were similar. After the hydrochloric acid treatment, the concentrations of many elements (Mo, V, and Ni) in the pyrobitumen changed slightly, whereas these of other elements, such as Ba, Sr, Cr, and Nb, significantly decreased.

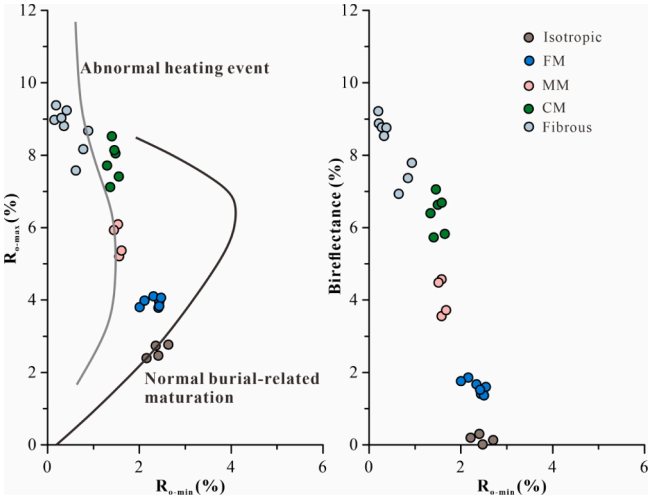

Fig. 8. Reflectance characteristics of the pyrobitumen with different optical textures (a) As the optical texture changes as isotropic → FM → MM → CM → fibrous, the maximum reflectance ($R_{o\text{-}max}$) gradually increases while the minimum reflectance ($R_{o\text{-}min}$) gradually decreases; MM, CM, and fibrous pyrobitumen samples fall near the baseline of the abnormal thermal event while isotropic, and FM pyrobitumen samples fall near the baseline of normal burial-related maturation; (b) As the optical texture changes as isotropic → FM → MM → CM → fibrous, the bireflectance increases gradually;

pyrobitumen pores and considered them authigenic barite related to hydrothermal activity. The apparent decrease in Ba concentrations after the treatment indicates that the Ba enrichment in pyrobitumen is in barite and other barium-enriched minerals. Combining the previous study results and the precipitation environment of illite and salt, these minerals that filled the pyrobitumen pores are of hydrothermal origin. The related hydrothermal fluids have high salinity (>18 wt% NaCl) and could pass through deep clastic strata during their upward migration [11,61] (Fig. 1b and c). Therefore, the hydrothermal fluids with high salinity and rich terrigenous materials provide precipitation conditions for salt and illite.

The precipitated barium-enriched minerals, illite, and salt carry numerous elements, remaining the trace of hydrothermal participation

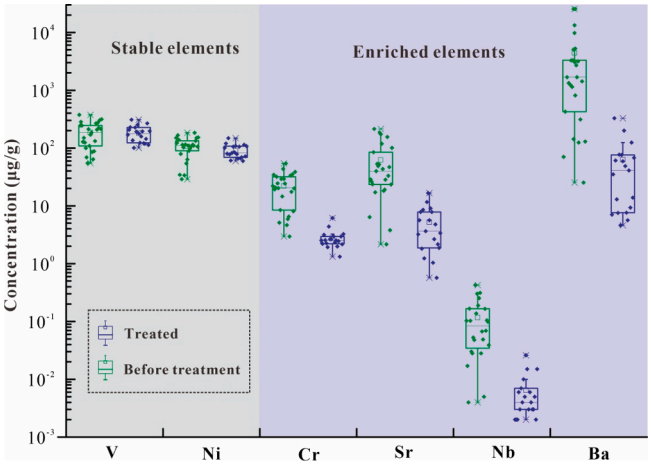

Fig. 9. Trace element changes of the pyrobitumen after hydrochloric acid treatment The concentrations of V and Ni are stable after hydrochloric acid treatment, whereasthose of Cr, Sr, Nb, and Ba decrease.

(Fig. 6). The trace element comparision in the pyrobitumen samples before and after treatment shows that Ba, Cr, Sr, and Nb in the untreated pyrobitumen samples are enriched (Fig. 9). The Ba enrichment is related to barium-enriched minerals, and the Cr enrichment could relate lamellar illite. The enrichment of these elements is closely related to hydrothermal minerals. Although EDS does not effectively measure some enriched elements (Sr and Nb), their concentrations positively correlate with those of Cr and Ba (Fig. 10). Therefore, these enriched elements could have the same source and are related to hydrothermal activities. However, the V and Ni concentrations before and after treatment are not significantly changed, indicating that the hydrothermal influence on these elements is limited, and they maintain the parent characteristics (Fig. 9). There are differences in the trace element compositions of the hydrothermal altered and normal pyrobitumen. These differences are more likely related to the precipitation of some hydrothermal minerals in the pyrobitumen pores. This discovery provides direct evidence for identifying the hydrothermally altered pyrobitumen.

5.3. *Optical texture and hydrothermal modification*

Identifying hydrothermally altered pyrobitumen has not attracted much attention, and most scholars only refer to the reflectance and optical texture of pyrobitumen for preliminary judgment [11]: [50]. Goodarzi (1993) first proposed this method when studying the pyrobitumen in the Baffin Island Nanisivik mine, Canada [63]. Concerning this chart, the MM, CM, and fibrous pyrobitumen samples in the study area fall near the abnormal thermal event line, indicating that they experience hydrothermal influence. The isotropic and FM pyrobitumen samples fall close to the normal burial-related maturation line, indicating that they come from the normal burial-related oil cracking (Fig. 8). The optical change of pyrobitumen is primarily controlled by aromatic lamellae order, representing the highest temperature the pyrobitumen experienced or its maturity. The maximum burial depth of the DY Formation can reach 7000–8000 m, and the corresponding formation temperature was 220–240 °C [37,66]. Although mesophase pyrobitumen is hard to form under 300 °C in the lab, many people speculate that a high burial temperature of 240 °C can promote the mesophase sphere precipitation and the formation of anisotropic pyrobitumen under the compensation of geological time. Therefore, it is unconvincing to identify the hydrothermally altered pyrobitumen simply from the optical texture and reflectance.

Hydrothermal activities enrich some elements in pyrobitumen, and conversely, the pyrobitumen enriched these elements could experience

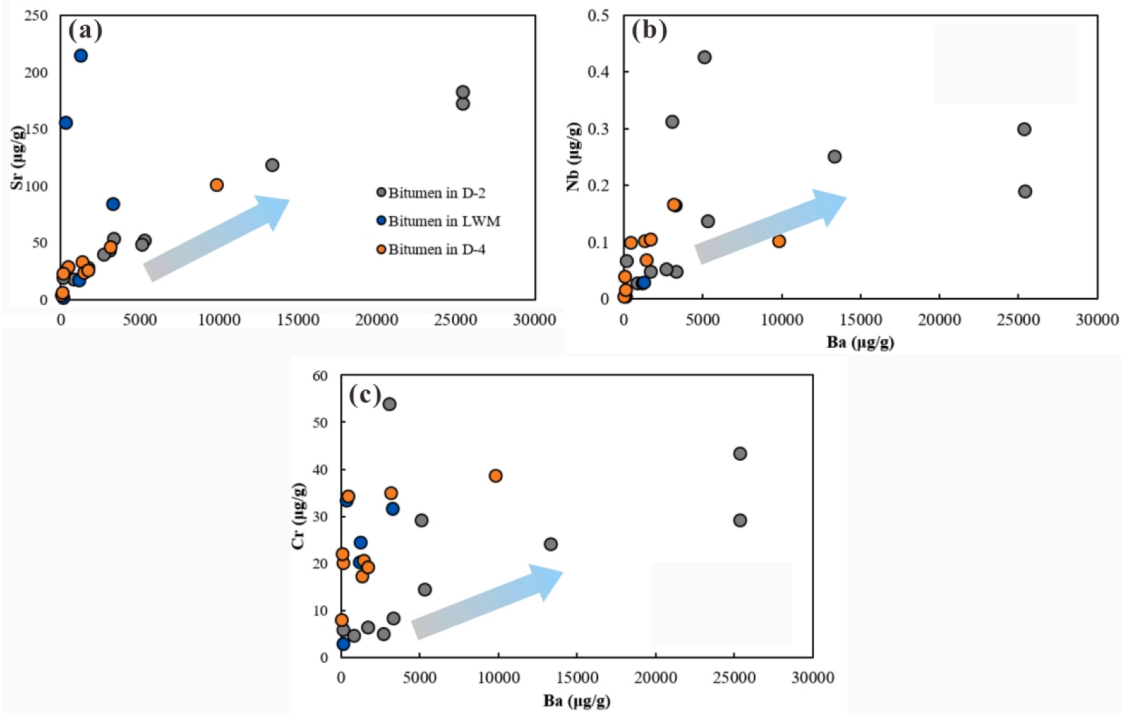

Fig. 10. Cross plot of trace elements in pyrobitumen (a–c) The concentrations of Sr, Nb, and Cr positively correlate with that of Ba; (d) The concentrations of V and Ni in pyrobitumen before and after hydrochloric acid treatment have similar distribution ranges.

hydrothermal modification. Since the hydrothermal activity has led to trace element enrichment while some elements retain their parent characteristics, the ratio of the two trace element sets can reflect the material exchange degree between pyrobitumen and hydrothermal modification. In this study, the most enriched elements (Ba, Sr, Nb, and Cr) are selected to characterize the material exchange degree, whereas V and Ni, which have a minor hydrothermal modification, are selected as the stable elements. The ratio of these two element sets can indicate the material exchange degree. Generally, these parameters can be combined to analyze the hydrothermal alteration degree of pyrobitumen (Fig. 11). It is suggested that the isotropic pyrobitumen in the study area primarily comes from the normal burial related oil cracking [11,58,61]. Fig. 11 shows that all parameters of isotropic pyrobitumen are extremely low, indicating that the element exchange between the pyrobitumen and hydrothermal fluid is the weakest. Therefore, this pyrobitumen has the slightest hydrothermal modification, consistent with a previous study [11]. The parameter values of different elements in the DY pyrobitumen are highly consistent with the optical textures. As the optical texture changes as FM → MM → CM → fibrous, each parameter gradually increases, indicating that the optical texture is closely related to the hydrothermal participation (Fig. 11). In essence, the optical texture of pyrobitumen has little to do with the participation of the materials in the hydrothermal fluid, but with the hydrothermal temperature. The hydrothermal influence on the optical texture of pyrobitumen can be realized by thermal conduction through the rocks or direct contact with the pyrobitumen. The study results of trace elements and optical texture support the latter, and the optical texture alteration correlate well with the trace element changes. Especially for fibrous pyrobitumen, various trace element parameters are all the highest (Fig. 11), indicating that the higher the material exchange degree between the pyrobitumen and hydrothermal fluid, the more orderly the aromatic lamellae in the pyrobitumen and the greater the graphitization degree. The DY Formation in the study area primarily comprises carbonate rocks deposited in bioherm beach facies. Under supergene karstification, the reservoir has good porosity and permeability, and two sets of high permeability weathering crusts are developed at the top of D-2 and D-4 members (Fig. 1c), providing a practical path for hydrothermal fluid and making it possible for the material exchange between hydrothermal fluid and pyrobitumen. Note that the trace element ratios of FM and MM pyrobitumen in the LWM Formation are higher than those of DY pyrobitumen with the same optical textures, indicating a sufficient material exchange and a lower temperature modification. The hydrothermal fluid must pass through the thick QZS Formation (Fig. 1c) during the upward migration through the DY Formation. Thus, a temperature loss occurs in the hydrothermal fluid in this migration; therefore, there is little fibrous pyrobitumen in the LWM Formation, and its distribution is limited [58].

Previous studies have found that hydrothermal activity can improve the porosity and permeability of the DY reservoir and promote the oil cracking of paleo-oil reservoirs [18,9,10]. These impacts are presumed to be confined near the deep faults due to the lack of hydrothermal scale studies. The optical textures and trace element concentrations of DY pyrobitumen confirm that a degree of material exchange occurred between anisotropic pyrobitumen and hydrothermal fluid in the DY Formation. As the optical texture changes as FM → MM → CM → fibrous, the material exchange and the hydrothermal alteration degrees increase. According to the plane view of pyrobitumen distribution, the MM, CM, and fibrous pyrobitumens dominate the central Sichuan Basin (Fig. 12), indicating that the hydrothermal activity is not limited to the faults but is widely developed. The entire central Sichuan area is affected by hydrothermal activity, whereas the hydrothermal modification degree varies in different regions. The highest hydrothermal temperature and modification are found in the Gaoshiti area, where fibrous pyrobitumen develops in the D-2 and D-4 members. The hydrothermal modification on the hydrocarbon accumulation of the DY Formation cannot be ignored.

6. Conclusion

Through the SEM, reflectance, and trace element analyses, this paper clarified the trace element concentrations and optical texture of hydrothermally altered pyrobitumen and discussed the hydrothermal scale and its geological significance in central Sichuan. The following

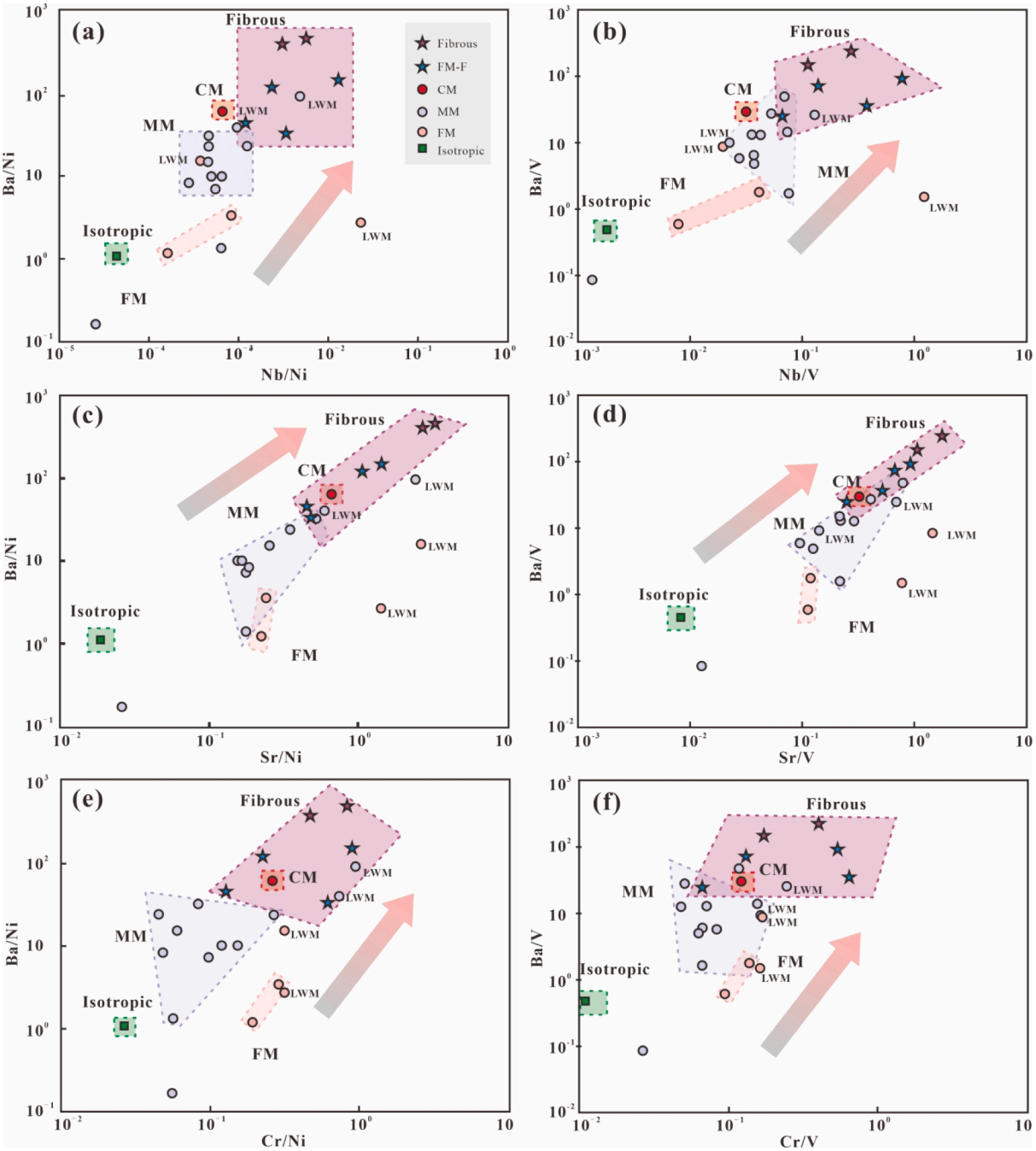

Fig. 11. The cross plots of concentration ratios between Ba, Cr, Sr, Nb, V, and Ni The concentration ratios between Ba, Cr, Nb, Sr, V, and Ni gradually increase as the optical textures of pyrobitumen change as isotropic → FM → MM → CM → fibrous. The element concentration ratios of the FM and MM pyrobitumen samples from the LWM Formation are higher than these of DY pyrobitumen with the same optical textures.

conclusions can be drawn:

Five optical pyrobitumen categories develop in the DY Formation: isotropic, FM, MM, CM, and fibrous. With the optical texture changes from isotropic to fibrous, the order degree of the aromatic lamella in the pyrobitumen and the pyrobitumen maturity gradually increase.

Affected by the hydrothermal fluid, the pyrobitumen pores are filled with authigenic illite, salt, and barium-enriched minerals, which could cause the Ba, Cr, Nb, and Sr enrichment in the hydrothermally altered pyrobitumen.

The hydrothermal alteration on pyrobitumen is primarily through direct contact. As the optical texture of the pyrobitumen changes as FM → MM → CM → fibrous, the element enrichment degree gradually increases.

The hydrothermal activity is not limited to the deep faults but develops in the entire central Sichuan Basin; therefore, hydrothermal modification on the reservoirs and paleo-oil reservoirs might occur in the entire central Sichuan Basin, which should be an essential part in the further studies on hydrocarbon accumulation.

This study identified the responses of trace elements and optical textures of ultra-deep pyrobitumen to hydrothermal alteration, and these responses were used to determine the hydrothermal range. It also provides a new method for hydrothermal studies in the deep strata, and helps specify the hydrothermal modification scale on deep hydrocarbon accumulation.

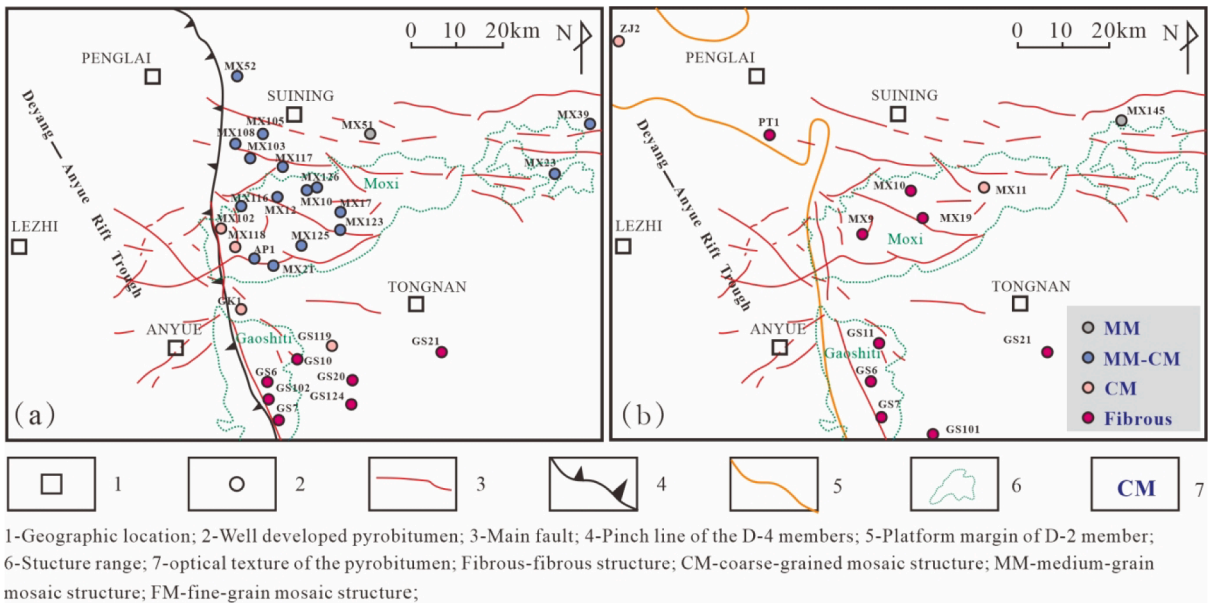

Fig. 12. Plane view of the pyrobitumen with different optical textures in the DY Formation The DY Formation is primarily filled with MM, CM, and fibrous pyrobitumens, indicating a large-scale hydrothermal modification not limited to the fractures. The fibrous pyrobitumen is observed in the D-2 and D-4 formations in the Gaoshiti area, representing the most vigorous hydrothermal modification in the study area.

CRediT authorship contribution statement

Lianqiang Zhu: Investigation, Writing – original draft. **Zezhang Song:** Funding acquisition, Project administration, Supervision, Writing – review & editing. **Xingwang Tian:** Validation, Project administration, Resources. **Guangdi Liu:** Writing – review & editing. **Dailin Yang:** Data curation, Resources. **Wenzhi Wang:** Data curation, Investigation. **Gang Zhou:** Conceptualization, Data curation. **Wei Yan:** Visualization, Data curation, Investigation. **Zhu Xiang:** Investigation. **Zili Zhang:** Investigation. **Qiang Li:** Investigation.

Declaration of Competing Interest

The authors declare that they have no known competing financial interests or personal relationships that could have appeared to influence the work reported in this paper.

Data availability

Data will be made available on request.

Acknowledgements

This research was financially supported by the National Natural Science Foundation of China (Grant NO. 42272161, Hydrothermal activities in deeply-buried and ultra-deeply-buried strata and the quantitative characterization of its alteration effect to paleo-oil-reservoir). We would also thank the PetroChina Southwest Oil and gas field Company for providing core samples and necessary data.

References

[1] Ban LL, Hess WM. Microstructure and morphology of carbon blacks. Petroleum Derived Carbons, ACS Symposium Series 1976;1976(21):358–77.
[2] Ban, L.L., Hess, W.M., 1971. A high-resolution electron microscopy study. Summary of Papers for 10th Biennial conference on Carbon. 1971, 98-99.
[3] Brooks JD, Taylor GH. Formation of graphitising carbons from the liquid phase. Nature 1965;3:697–9.
[4] Chen X, Zhao WZ, Zhang LP, Zhao ZJ, Liu YH, Zhang BM, et al. Discovery and exploration significance of structure-controlled hydrothermal dolomites in the Middle Permian of the central Sichuan Basin. Acta Pet Sin 2012;33(4):562–9.
[5] Du JH, Zhang BM, Wang ZC, Zou CN, Xu CC, Shen P, et al. The carbonate gentle slope of the Lower Cambrian Longwangmiao Formation in the Sichuan Basin Sedimentary model and reservoir genesis of grain beach. Nat Gas Ind 2016;36:1–10.
[6] Du JH, Zou CN, Xu CC, He HQ, Shen P, Yang YM, et al. Strategic discovery and theoretical technology innovation of the Longwangmiao Formation extra-large gas field in the central Sichuan paleo-uplift. Pet Explor Dev 2014;41:268–77.
[7] Eksilioglu A, Gencay N, Yardim MF. Mesophase AR pitch derived carbon foam: Effect of temperature, pressure and pressure release time. J Mater Sci 2006;41:2743–8.
[8] Fathollahi, B., Jones, B., Chau, P.C., 2005. Injection and stabilisation of mesophase pitch in the fabrication of carbon-carbon composites. PartIII: Mesophase stabilisation at low temperatures and elevated oxidation pressures. Carbon. 2005, 43, 143-151.
[9] Feng MY, Qiang ZT, Shen P, Zhang J, Tao YZ, Xia ML. Evidences for hydrothermal dolomite of Sinian Dengying Formation in Gaoshiti-moxi area Sichuan Basin. Acta Pet Sin 2016;37(5):587–98.
[10] Feng MY, Wu PC, Qiang ZT, Liu XH, Duan Y, Xia ML. Hydrothermal dolomite reservoir in the Precambrian Dengying Formation of central Sichuan Basin, Southwestern China. Mar Pet Geol 2017;82:206–19.
[11] Gao P, Liu GD, Lash GG, Li BY, Yan DT, Chen C. Occurrences and origin of reservoir solid bitumen in Sinian Dengying Formation dolomites of the Sichuan Basin, SW China. Int J Coal Geol 2018;200:135–52.
[12] Gleb S, Pokrovski MB, Gaëlle S, Franck P. Mechanisms and rates of pyrite formation from hydrothermal fluid revealed by iron isotopes. Geochim Cosmochim Acta 2021;304:281–304.
[13] Grint A, Swietlik U, Marsh H. Carbonisation and liquid-crystal (mesophase) development. The co-carbonisation of vitrains with Ashland A200 petroleum pitch. Fuel 1979;58:642–50.
[14] Hatshorme NH. The microscopy of liquid crystals, monographs in microscopic series. London: Microscope Publications; 1974.
[15] Heidenreich RD, Hess WM, Ban LL. A test object and criteria for high resolution electron microsopy. J Appl Cryst 1968;1:1–19.
[16] Huang KN, Opdyke ND. Magnetostratigraphic investigations on an Emeishan basalt section in western Guizhou province. China Earth & Planetary Science Letters 1998;163(1–4):1–14.
[17] Jiang YQ, Gu YF, Zhu X, Xu W, Xiao R, Li JL. Hydrothermal dolomite reservoir facies in the Sinian Dengying Fm. Central Sichuan Basin Natural Gas Industry 2017;37(3):17–24.
[18] Jiang YQ, Tao YZ, Gu YF, Wang JB, Qiang ZT, Jiang N, et al. Hydrothermal dolomitization in Sinian dengying formation, gaoshiti-moxi area, sichuan basin, SW China. Petrol Explor Dev 2016;43(1):51–60.
[19] John A, Groff. Fluid evolution during Cretaceous and Eocene igneous–Hydrothermal events in the Getchell trend. Nevada Ore Geol. Rev. 2021;137:104303.
[20] Li SJ, Yang TB, Han YQ, Gao P, Wo YJ, He ZL. Hydrothermal dolomitization and its role in improving Middle Permian reservoirs for hydrocarbon accumulation. Sichuan Basin Oil Gas Geol. 2021;42(6):1265–80.
[21] Luo B, Luo WJ, Wang WZ. The formation mechanism of Sinian gas reservoirs in Leshan-Longnüsi paleo-uplift. Sichuan Basin Nat. Gas Geosci. 2015;26(03):444–55.

[22] Luo B, Yang YM, Luo WJ, Wen L, Wang WZ, Chen K. Controlling factors and distribution of reservoir development in Dengying Formation of paleouplift in central Sichuan Basin. Acta Pet Sin 2015;36(04):416–26.
[23] Luo Q, Hao J, Skovsted CB, Luo P, Khan I, Wu J, et al. The organic petrology of graptolites and maturity assessment of the Wufeng-Longmaxi formations from Chongqing, China: insights from reflectance cross-plot analysis. Int J Coal Geol 2017;183:161–73.
[24] Luo QY, Zhong NN, Dai N, Zhang W. Graptolite-derived organic matter in the Wufeng-Longmaxi Formations (Upper Ordovician-Lower Silurian) of southeastern Chongqing, China: implications for gas shale evaluation. Int J Coal Geol 2016;153:87–98.
[25] Ma, Y.S., Ni, M.W., Cai, X.Y., Xu, X.H., Hu, D.F., Qu, S.L., Li, G.S., 2021. Advances in basic research on the mechanism of deep marine hydrocarbon enrichment and key exploitation technologies. 43(05), 737-748 (in Chinese).
[26] Marsh H. Carbonization and liquid-crystal (mesophase) development: part 1. The significance of the mesophase during carbonisation of coking coals. Fuel 1973;52:205–12.
[27] Parnell J, Baron M, Mann P, Carey P. Oil migration and bitumen formation in a hydrothermal system. Cuba Journal of Geochemical Exploration 2003;78–79:409–15.
[28] Patrick JW, Reynolds MJ, Shaw FH. Development of optical anisotropy in vitrains during carbonisation. Fuel 1973;52:198–204.
[29] Ran QG, Cheng HG, Xiao ZY. Structural thermal events in Tadong area and their impact on crude oil cracking. Mod Geol 2008;2008(04):541–8. in Chinese.
[30] Rimmer SM, Crelling JC, Yoksoulian LE. An occurrence of coked bitumen, Raton Formation, Purgatoire River Valley, Colorado, U.S.A. Int J Coal Geol 2015;141–142:63–73.
[31] Sanada Y. Utilisation of heavy oil carbonisation and carbon materials. J Fuel Soc Jpn 1978;57:117–31.
[32] Shan XQ, Zhang J, Zhang BM, Liu JJ, Zhou H, Wang YJ, et al. Characteristics of dolomite karst reservoirs in the Sinian Dengying Formation in the Sichuan Basin and evidence of dissolution. Acta Pet Sin 2016;37:17–29.
[33] Shen AJ, Hu AP, Cheng T, Liang F, Pan WQ, Feng YX, et al. Laser in-situ U-Pb isotope dating technology and its application in carbonate diagenesis and pore evolution. Pet Explor Dev 2019;46:1062–74.
[34] Shen AJ, Zhao WZ, Hu AP, Wang H, Liang F, Wang YS. Carbonate mineral dating and temperature fixation technology and its application in the study of oil and gas accumulation in the central Sichuan paleo-uplift. Pet Explor Dev 2021;48:476–87.
[35] Shen ZM. New carbon materials. Beijing: Chemical Industry Press; 2003. in Chinese.
[36] Stasiuk LD. The origin of pyrobitumens in upper Devonian Leduc formation gas reservoirs, Alberta, Canada: an optical and EDS study of oil to gas transformation. Marine Petrol Geol 1997;14:915–29.
[37] Su A, Chen HH, Feng YX, Zhao JX, Nguyen AD, Wang ZC, et al. Dating and characterising primary gas accumulation in Precambrian dolomite reservoirs, Central Sichuan Basin, China: Insights from pyrobitumen Re-Os and dolomite U-Pb geochronology. Precambr Res 2020;350:105897.
[38] Sun SS, Yu H, Xu YL, Wu L, Zhu YM, Zhao XF. Preparation and characterisation of high softening point coated asphalt. Appl Chem Ind 2020;49:2437–41.
[39] Wei GQ, Xie ZY, Song JR, Yang W, Wang ZH, Li J, et al. Sinian-Cambrian natural gas characteristics and genesis of the central Sichuan paleo-uplift in the Sichuan Basin. Pet Explor Dev 2015;42:702–11.
[40] White, J.L., 1976. Mesophase mechanisms in the formation of the microstructure of petroleum coke // Deviney, M.L., O'Grady, T.M. Petroleum Derived Carbons: American Chemical Society. 282-314.
[41] White JL, Price RJ. The formation of mesophase microstructures during the pyrolysis of selected coker feedstocks. Carbon 1974;12:321–33.
[42] Wilson NSF. Organic petrology, chemical composition, and reflectance of yrobitumen from the El Soldado Cu deposit. Chile Int J Coal Geol 2000;43:53–82.
[43] Xie ZY, Li J, Yang CL, Tian XW, Zhang L. Geochemical characteristics of Sinian-cambrian natural gas in central Sichuan paleo-upliftand exploration potential of Taihe gas area. Nat Gas Ind 2021;71(7):1–14.
[44] Xu CC, Shen P, Yang YM, Luo B, Huang JZ, Jiang XF, et al. The natural gas accumulation conditions and enrichment rules of the Sinian-Lower Cambrian Longwangmiao Formation in the Leshan-Longnüsi paleo-uplift. Nat Gas Ind 2014;34:1–7.
[45] Yamada Y, Imamura T, Kakiyama H. Characteristics of meso-carbon microbeads separated from pitch. Carbon 1974;12:307–19.
[46] Yang CY, Li MJ, Ni ZY, Wang TG, Qiu NS, Fang RH, et al. Paleo-oil reservoir pyrolysis and gas release in the Yangtze Block imply an alternative mechanism for the Late Permian Crisis. Geosci Front 2022;13(2):101324.
[47] Yang CY, Ni ZY, Li MJ. Pyrobitumen in South China: Organic petrology, chemical composition and geological significance. Int J Coal Geol 2018;188:56–63.
[48] Yokono T, Yamada J, Sanada Y. Formation of carbon microbeads from paraffin / pitch systems under mild pressure and temperature conditions. J Mater Sci Lett 1986;5:779–80.
[49] J.C. Zhang H.K. Nie B. Xu S.L. Jiang P.X. Zhang Z.Y. Wang Geological condition of sahle gas accumulation in Sichuan Basin Nature Gas Industry. 2008 02 2008 151–156+179-180.
[50] Zhang PW. Study on the genesis mechanism of hydrogen sulfide in Sinian Cambrian gas reservoir in Central Sichuan region. University of petroleum of China (Beijing); 2019.
[51] Zheng P, Shi YY, Zou CY, Kong LM, Wang LS, Liu JZ. Analysis of natural gas source of Dengying Formation and Longwangmiao Formation in Gaoshiti-Moxi area. Nat Gas Ind 2014;34:50–4.
[52] Zhong YT, He B, Mundil R. CA-TIMS zircon U-Pb dating of felsic ignimbrite from the Binchuan section: Implications for the termination age of Emeishan Large Igneous Province. Lithos 2014;204(03):14–9.
[53] Zhou JG, Zhang JY, Deng HY, Chen YN, Hao Y, Li WZ, et al. Lithofacies paleogeography and sedimentary model of the Sinian Dengying Formation in Sichuan Basin. Nat Gas Ind 2017;37:24–31.
[54] Zhu DY, Jin ZJ, Hu WX. Influence of abnormal thermal action on crude oil in paleo-reservoir—Taking Well Tazhong 18 in Tarim Basin as an example. Earth Sci 2008;38(03):294–306. Science in China (Series D:(in Chinese.
[55] Zhu GY, Wang TS, Xie ZY, Xie BH, Liu KY. Giant gas discovery in the Precambrian deeply buried reservoirs in the Sichuan Basin, China: implications for gas exploration in old cratonic basins. Precambr Res 2015;262:45–66.
[56] Zhu GY, Zhang SC, Yang YB, Ma YS, Dai JX, Li J, et al. The characteristics of natural gas in sichuan basin and its sources. Earth Sci Front 2006;2006(02):234–48.
[57] Zhu LQ, Liu GD, Song ZZ, Zhao WZ, Li Q, Tian XW, et al. Reservoir solid bitumen-source rock correlation using the trace and rare earth elements–implications for identifying the natural gas source of the Ediacaran-Lower Cambrian reservoirs, central Sichuan Basin. Mar Pet Geol 2022;137:105499.
[58] Zhu LQ, Liu GD, Song ZZ, Zhang BJ, Zhao WZ, Tian XW, et al. Hydrothermal activity in ultra-deep strata and its geological significance for deep earth gas exploration: Implications from pyrobitumen in the Ediacaran-lower Cambrian Strata, Sichuan Basin. Int J Coal Geol 2022;259:104030.
[59] Zou CN, Du JH, Xu CC, Wang ZC, Zhang BM, Wei GQ, et al. Formation, distribution, resource potential and discovery of the Sinian-cambrian giant gasfield, Sichuan Basin, SW China. Pet Explor Dev 2014;41(03):278–93.
[60] Zou CN, Wei GQ, Xu CC, Du JH, Xie ZY, Wang ZC, et al. Geochemistry of the Sinian-Cambrian gas system in the Sichuan Basin, China. Org Geochem 2014;74:13–21.
[61] Zhang PW, Liu GD, Cai CF, Li MJ, Chen RQ, Gao P, et al. Alteration of solid bitumen by hydrothermal heating and thermochemical sulfate reduction in the Ediacaran and Cambrian dolomite reservoirs in the Central Sichuan Basin, SW China. Precambr Res 2019;321:277–302.
[62] Shi CH, Cao J, Selby D, Tan XC, Luo B, Hu WX. Hydrocarbon evolution of the over-mature Sinian Dengying reservoir of the Neoproterozoic Sichuan Basin, China: Insights from Re–Os geochronology. Mar Pet Geol 2020;122:104726.
[63] Goodarzi F. Optical Characteristics of Heat-Affected Bitumens from the Nanisivik Mine, N.W. Baffin Island. Arctic Canada. Energy Sources 1993;15:359–76.
[64] Song ZZ, Liu GD, Luo B, Zeng QC, Tian XW, Dai X, et al. Logging evaluation of solid bitumen in tight carbonate in deep-buried and ultra-deep-buried strata of the central Sichuan Basin. Acta Sedimentolo Sin 2020;39:197–211.
[65] Yang CY, Li MJ, Wang TG, Zhong NN, Fang RH. Texture development of mesophase in reservoir pyrobitumen and the temperature-pressure converting of the gas reservoir in the Chuanzhong Uplift, Southwestern China. Petroleum Sci 2022 (in press).
[66] Song ZZ, Ding XH, Zhang BJ, Ge BF, Tian XW, Chen X, et al. Dynamic reconstruction of the hydrocarbon generation, accumulation, and evolution history in ultra-deeply-buried strata. Front Earth Sci 2022;10.